Acoustic Streaming for Flow Manipulation and Control

Christopher Stone*, Luke Bowen†, Bruce Drinkwater‡, Anthony Croxford§ and Mahdi Azarpeyvand¶
Faculty of Engineering, University of Bristol, BS8 1TR, UK

The effect of bulk-driven acoustic streaming on a turbulent boundary layer over a flat plate has been experimentally measured. In this fundamental study for boundary layer manipulation, the acoustic streaming flows were induced by two different types of high power ultrasonic transducers: a Langevin horn and a focussed array of parking sensor transducers, operating at 26 kHz and 40 kHz respectively. The boundary layer was characterised using CTA hot-wire anemometry, with high resolution measurements recorded in both the streamwise and spanwise directions around the transducer location. The results show that acoustic streaming flows in the order of 1.5 m/s can cause a reduction in the velocity energy content of approximately 3 dB across a wide frequency range between 10 Hz and 8 kHz.

I. Nomenclature

C_p	=	Coefficient of pressure
d	=	Hole diameter [m]
f	=	Frequency [Hz]
f_s	=	Transducer operating frequency [Hz]
H	=	Height [m]
L	=	Streamwise length of flat plate [m]
l_h	=	Length of Langevin horn [m]
p	=	Static pressure [Pa]
p_∞	=	Free-stream static pressure [Pa]
Re_d	=	Reynolds number
r	=	Radial co-ordinate [m]
r_f	=	Focal length of focussed array [m]
U_∞	=	Free-stream velocity [m/s]
$\bar{U}$	=	Mean velocity [m/s]
u'	=	RMS velocity [m/s]
U_s	=	Acoustic streaming velocity [m/s]
W	=	Width [m]
x	=	Streamwise co-ordinate [m]
y	=	Spanwise co-ordinate [m]
z	=	Wall normal co-ordinate [m]
δ	=	Boundary layer thickness [m]
ρ	=	Fluid density [kg/m^3]
ϕ_{ii}	=	Power spectral density of variable i [dB/Hz]
BL	=	Boundary Layer
CTA	=	Constant Temperature Anemometry
PSD	=	Power Spectral Density
RMS	=	Root Mean Square
SPL	=	Sound Pressure Level [dB]
TI	=	Turbulence Intensity

*PhD student, Department of Mechanical Engineering, University of Bristol, c.stone@bristol.ac.uk
†Post-doctoral Research Associate, Department of Mechanical Engineering, University of Bristol, luke.bowen@bristol.ac.uk
‡Professor of Ultrasonics, Department of Mechanical Engineering, University of Bristol, b.drinkwater@bristol.ac.uk
§Professor of Ultrasonics and Dynamics, Department of Mechanical Engineering, University of Bristol, a.j.croxford@bristol.ac.uk
¶Professor of Aerodynamics and Aeroacoustics, Department of Mechanical Engineering, University of Bristol, m.azarpeyvand@bristol.ac.uk

II. Introduction

Flow control methods for boundary layer manipulation have long been the subject of extensive research due to the wide range of benefits that can be realised. Delaying flow separation, drag reduction and flow-induced noise suppression are but a few examples of the advantages of flow control. Many different passive flow control approaches have been formulated including serrated edges [1, 2], porous materials [3, 4] and surface treatments [5, 6] which manipulate the flow without an external energy input.

More recently, active methods such as flow injection [7–9], flow suction [10–12] and plasma actuation [13] have been proposed, all of which have been shown to alter the characteristics of vortical structures within turbulent boundary layers. Flow injection treatments displace the structures away from the surface, creating a layer of fluid characterised by low energy content. Blowing in both perpendicular [8] and inclined [9] orientations has been studied, and both decouple the velocity and surface pressure fluctuations. One disadvantage associated with perpendicular blowing is the flow separation it can cause, a common solution for separation is to incline the jets. Flow suction on the other hand breaks larger vortices up via the increase in viscous diffusion as the structures are pulled closer to the surface. Here, a novel active method is proposed, using bulk-driven acoustic streaming to manipulate a turbulent boundary over a flat plate.

Acoustic streaming is a second order effect, where the attenuation of acoustic energy generates time-independent fluid flows. The phenomenon was first investigated by Rayleigh in the late 19^{th} century [14] where rotational flows were observed in a standing wave between two parallel plates. Rayleigh lends his name to these rotational flows, which were subsequently found to be driven by counter-rotating flows within the viscous (acoustic) boundary layer, known as Schlichting streaming [15]. As a result, Rayleigh-Schlichting streaming is the term commonly used to describe acoustic streaming that is generated from within the viscous boundary layer. Boundary layer-driven streaming has been widely studied, particularly within the field of microfluidics; applications such as particle separation [16, 17] and heat transfer enhancement [18, 19] are becoming increasingly popular, and accurate numerical models have been developed [20].

The focus in this work was on acoustic streaming that is driven by acoustic attenuation in the bulk of the fluid, often referred to as Eckart streaming [21], where the streaming takes the form of a jet flowing in the direction of the acoustic propagation. Eckart neglected the inertial terms in the Navier-Stokes equations to simplify the problem (an assumption previously used in studies on boundary layer-driven streaming by Rayleigh [14], Nyborg [22, 23] and Westervelt [24]), which Stuart proposed limited his analysis to very low velocity streaming flows induced by low power acoustic sources ($< 4 \times 10^{-4}$ W) [25]. For higher power sources, Stuart determined that the convective acceleration term in the Navier-Stokes equations (i.e. the inertial term) cannot be ignored; Lighthill stated that all 'clearly visible' streaming flows were a form of Stuart streaming [26]. Despite the limitations of Eckart's analyses, this type of acoustic streaming bears his name since he was the first to observe the mechanism for which the streaming flows are generated.

Compared to Rayleigh-Schlichting streaming, there have been very few practical utilisations of Eckart streaming. Hasegawa *et al.* used a phased array of ultrasonic transducers to create a steerable air flow induced by a Bessel beam [27] and subsequently a curved acceleration path in approximately 1 m of open air [28]. The authors themselves state that one possible reason for a lack of Eckart streaming applications in air is that conventional sound sources cannot provide the acoustic intensity required to generate the driving forces for acoustic streaming. Research into the numerical modelling of bulk-driven streaming has been limited to streaming in liquids [29], but at the time of writing no accurate airborne Eckart streaming model has been developed.

In the present study, the effect of Eckart streaming on a turbulent boundary layer is studied, using two different ultrasonic transduction methods: Langevin horns and a focussed array of parking sensor transducers. These devices are capable of producing the necessary acoustic pressures required to induce observable Eckart streaming flows in air, and are described in detail in Section III. Their effect on a turbulent boundary layer over a flat plate is quantified using hot-wire anemometry, with the experimental methods described in Section IV and the results presented in Section V.

III. Transduction setup and methods

In this section an overview of the transduction methods is presented, along with an experimentally validated computational model of the acoustic fields to be implemented for boundary layer modification.

A. Overview

To generate significant acoustic streaming flows in air, high attenuation and high acoustics pressures are required. Since the attenuation coefficient increases with the square of the acoustic frequency, ultrasonic transducers are certainly the best devices to achieve this aim. However, transduction methods capable of outputting the necessary high pressures that are currently available limit the acoustic frequency that can be achieved. In these experiments, two different

transduction methods were used: Langevin horns and focussed arrays of parking sensor transducers, the details of which are outlined in Table 1. Figure 1 shows an image of the two devices.

Table 1 Properties of ultrasonic transducers.

Transducer	f_s [kHz]	SPL (at z = 50 mm)* [dB]	Focal distance [mm]
Langevin horn	~26	148.3	<2
Focussed array	40	147.8	38

*50 mm away from the Langevin horn face, 50 mm away from the focussed array's focal point.

Langevin horns are half-wavelength resonators, consisting of an aluminium 'horn', a brass backing mass and a stack of piezoelectric rings, sandwiched together by a bolt tightened to a torque of 7 Nm. When resonating in the desired mode, the sound field produced is similar to that of a dipole source, and prior testing has shown that the Langevin horn face does indeed vibrate uniformly; this means the Langevin horn can be thought of as a very high powered piston source. During operation, the piezoelectric material heats up, causing the resonant frequency of the structure to change. As such, they must undergo a 'warm up' procedure so the resonance reaches a steady state ($f_s \approx 26$ kHz) to ensure the output is consistent during wind tunnel experiments. The resonant frequency of Langevin horns is very sensitive to the assembly of the devices, as well as environmental conditions such as the ambient air temperature.

Fig. 1 Image of a Langevin horn (left) and focussed array (right).

Conversely, the focussed array used here was made from 38 Murata MA40S4S ultrasonic sensors, often referred to as 'parking sensor transducers'. It was designed such that the focal point SPL would be similar to the peak SPL achieved by the Langevin horn. Since the transducers are mass produced and are not driven at the same high voltages as the Langevin horns, they are much more reliable in their operation: the acoustic output is consistent at a frequency of f_s = 40 kHz. The transducers fit into a 3D printed structure so the focal distance (i.e. the distance between each transducer face and the focal point) was r_f = 38 mm.

B. Modelling

Figure 2 shows the predicted SPL for both transducers in an axi-symmetric COMSOL Multiphysics model, illustrating the acoustic fields that these devices produce to understand what drives the acoustic streaming flows. A pressure acoustics model was used, with velocity conditions on boundaries to represent the transducer faces. The Langevin horn is a piston source and thus can be represented by a horizontal velocity condition boundary. A curved velocity condition boundary was used to model the focussed array, with a wall boundary condition implemented to represent the flat plate with a hole that allows the acoustic field to penetrate the boundary layer. It was found the presence of the hole changed the shape of the focussed array's acoustic field from a divergent profile to that of a dipole source - similar to the acoustic field produced by the Langevin horn. A spherical wave radiation condition was utilised on the outer boundary to allow acoustic waves to leave the air domain without reflection.

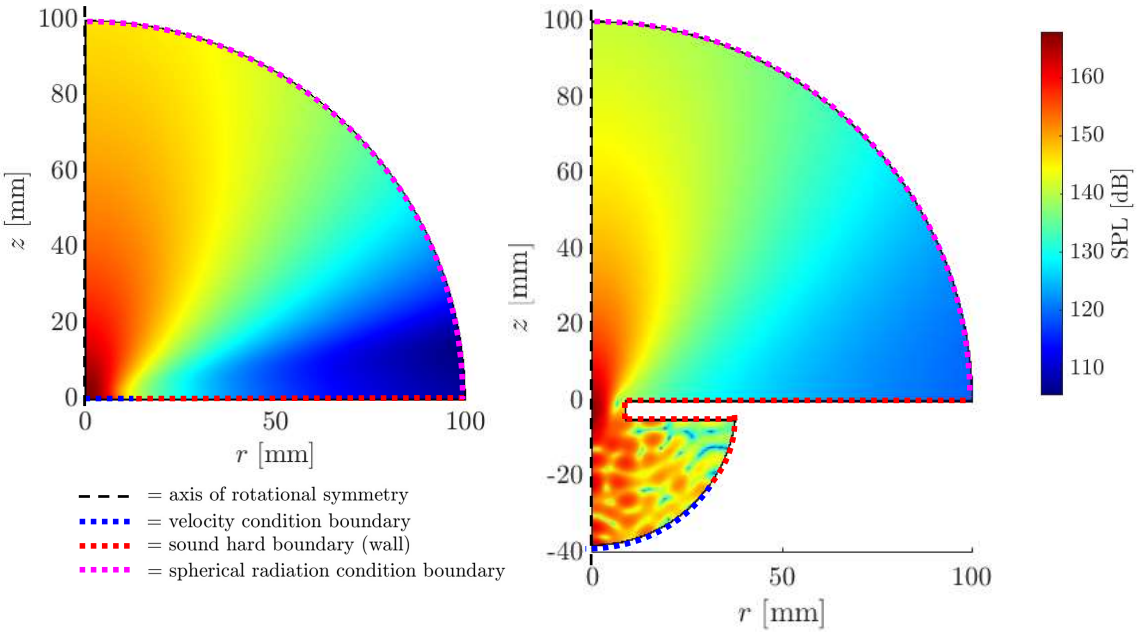

Fig. 2 Predicted acoustic fields of the Langevin horn (left) and focussed array (right).

The acoustic fields of the transducers were measured with a Brüel & Kjær Type 4138 1/8" Pressure-Field Microphone, which was mounted to a 3 axis traverse in order for the full acoustic field to be characterised experimentally. The magnitudes of the velocity conditions used in each transducer model were scaled such that the predicted axial pressure (along the z axis at $r = 0$) matched experimental measurements between $z = 50$ mm and $z = 100$ mm. Near-focus measurements were unable to be taken due to the extremely high acoustic pressures that would damage the microphone. Experimental measurements in the rz-plane showed excellent agreement with the COMSOL models.

Figure 2 shows that the acoustic field produced by the Langevin horn and arrays both have a similar peak acoustic pressure of approximately 167 dB. The peak pressure occurs very close to the velocity condition boundary for the Langevin horn model, while the focussed array field shows a focal spot in the centre of the hole in the flat plate. Above the plate surface, the acoustic field of the focussed array looks similar to that of the Langevin horn, although the acoustic beam has a higher directivity due to the higher frequency (40 kHz compared to 26 kHz) which results in a smaller focal region. Below the plate surface, the focussed array field displays interference patterns, representing how the acoustic fields from each individual parking sensor transducer interact with each other before the focal point. In the far field, the focussed array field decays faster than that of the Langevin horn. For the purpose of generating acoustic streaming flows, the volume of air that is subject to the highest acoustic pressure is the main factor, rather than lower pressures elsewhere in the field.

IV. Flat plate setup

In this section an overview of the measurement setup is shown, and further detail is given about how the transducers were mounted to maximise the effect of the acoustic streaming flows.

A. Flat plate measurements

Experimental measurements were performed in the University of Bristol's Pressure Neutral Wind Tunnel (PNWT), which is an open-jet anechoic wind tunnel with nozzle dimensions of $W = 995$ mm and $H = 775$ mm (see Fig. 3). Flow velocities were varied between $U_\infty = 10$ and $U_\infty = 15$ m/s to understand the effect of constant streaming on the boundary layer at multiple velocities. The flow velocities correspond to a range of Reynolds numbers between $Re_d = 1.2 \times 10^4$ and $Re_d = 1.8 \times 10^4$ (taking the hole diameter d as the characteristic length).

The plate was designed with a length of $L = 1690$ mm to generate a large boundary layer at the location of acoustic streaming. The streaming location, $x = 0$ mm, was positioned sufficiently far downstream for a large boundary layer to

develop, without being too close to the trailing edge to avoid interactions affecting measurements ($x/L = -0.973$). To ensure a turbulent boundary layer over the streaming location on the flat plate, zig-zag tape was applied to the surface of the plate next to the inlet.

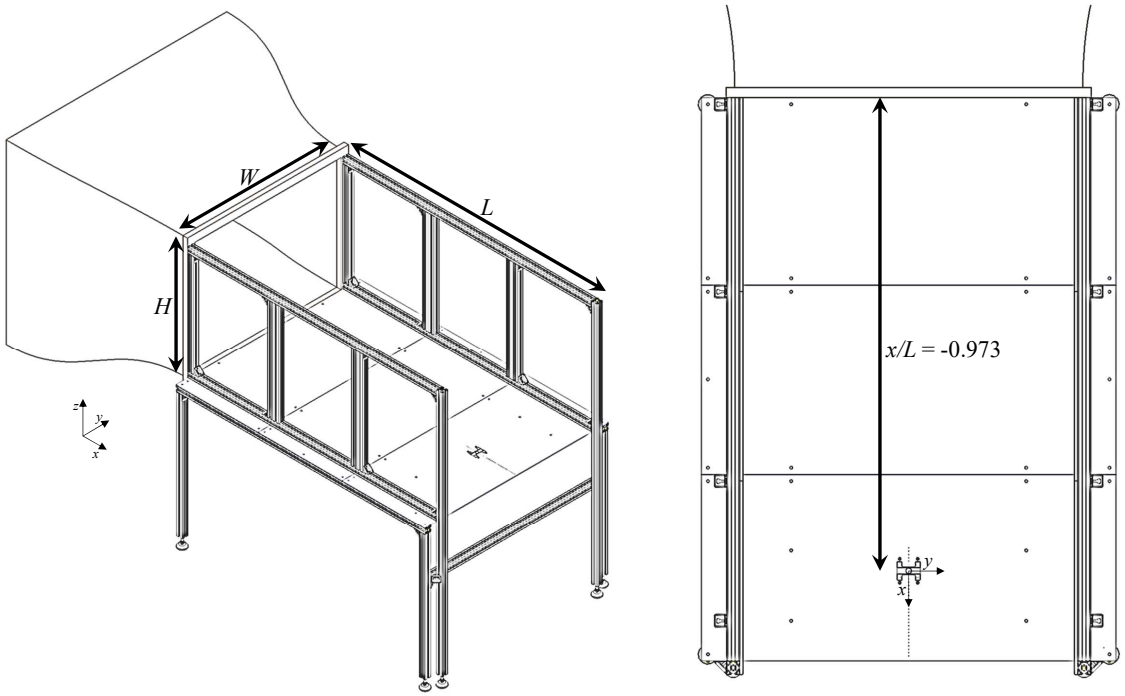

Fig. 3 Flat plate rig schematic.

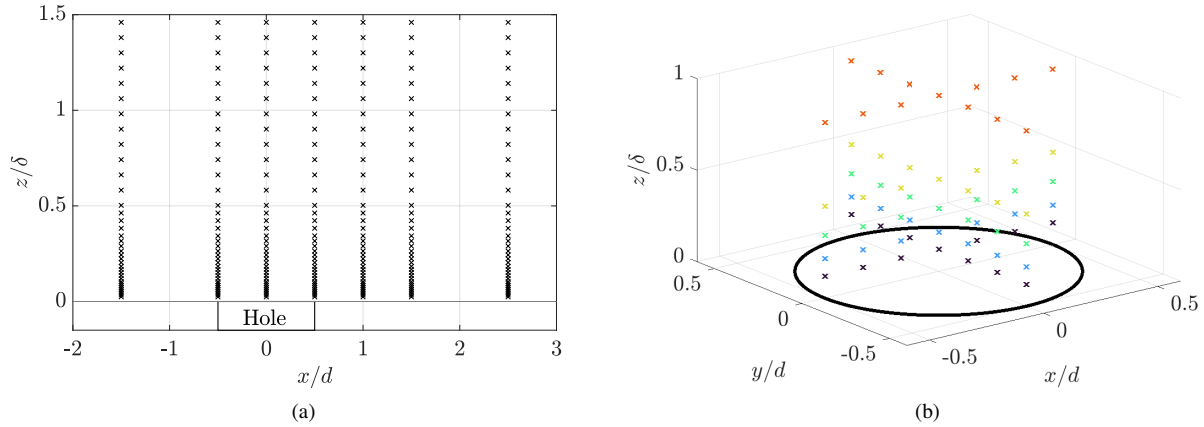

Fig. 4 Hot-wire anemometer measurement points for (a) full BL capture at $y/\delta = 0$ and (b) xz- and yz-plane scans over the hole.

Constant temperature anemometry (CTA) was used to characterise the boundary layer at multiple streamwise and spanwise locations (see Fig. 4). A Dantec 55P15 single-wire boundary layer probe was controlled by a Dantec Streamline Pro system with a CTA91C10 module, and was mounted to three (x, y, z) ThorLabs LTS300 300 mm translation stages. Data was collected for 16 s at a sampling rate of 2^{15} Hz at each measurement position. The hot-wire probe was calibrated using a Dantec 54H10 calibrator. First, a coarse scan was conducted in the z direction to find the

boundary layer thickness, defined as the height at which the mean velocity is 99% of the freestream velocity (found to be $\delta \approx 35$ mm at the streaming location, $x = 0$ mm), which determined the fine measurement locations shown in Fig. 4a to capture sufficient information, particularly close to the plate surface. Figure 4b shows the measurement locations following the full BL capture, with selected z/δ values chosen based on the previous results to measure in both the streamwise and spanwise locations around the transducer hole. Static pressure measurements were made along the streamwise direction ($y = 0$ mm) around the streaming location, using flush-mounted brass tubes which were glued in place. There were 30 pressure taps in total (6 upstream of the transducer hole, 24 downstream) with data obtained using a Chell MicroDaq-32 pressure acquisition system, sampling for 16 s at 312 Hz.

The plate was also instrumented with 48 Knowles FG-23329-P07 flush-mounted microphones in order to capture the surface pressure fluctuations. The microphones were calibrated for phase and amplitude using the same method as previously described in the literature [30, 31]. Microphones were placed on the centreline of the plate ($y = 0$ mm), with three upstream of the streaming location and 25 downstream until the trailing edge to observe the development of the boundary layer. Spanwise arrays of microphones were also employed near the transducer location to understand how streaming affected the spanwise coherence of turbulent structures.

B. Transducer mounting

The maximum acoustic streaming velocity will occur just beyond the peak acoustic pressure, therefore for these experiments it was important to arrange the transducers such that this peak velocity occurred within the boundary layer. Figure 5 displays the differences in mounting layouts for the two transducers: the Langevin horn could be mounted effectively flush with the flat plate surface, whereas the focussed array had to be further below the surface such that the focal point was located at the flat plate surface. In order to allow the acoustic field to penetrate the turbulent boundary layer of the flat plate, an aluminium mounting plate with a hole at the centre was created. Acoustically transparent mesh covered the hole to reduce the effects of the cavity whilst minimising the impact on the acoustic field of the transducers.The mesh is attached to grooves on the mounting plate, as seen in Fig. 5. It should be noted that the differences in geometries between the Langevin horn and the focussed array meant that the flow was affected by the cavity behind the mesh for the focussed array tests. For the Langevin horn there was little change in boundary layer profile.

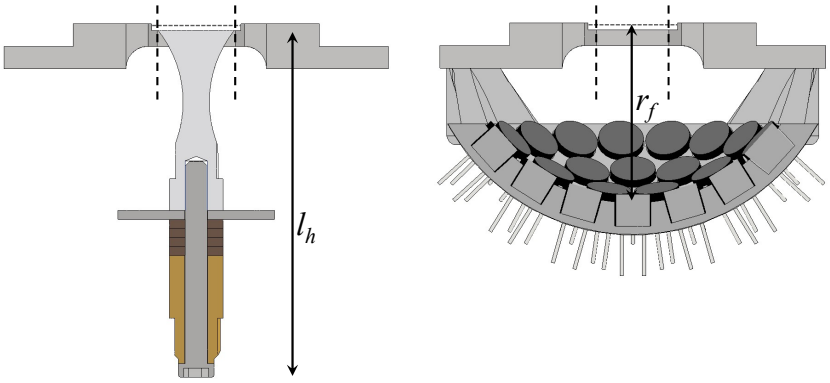

Fig. 5 Cross-section schematics of the Langevin horn (left) and focussed array (right) in the flat plate mount, with the hole limits indicated by the black dashed lines.

V. Results and discussion

Here the static pressure and hot-wire anemometry data is presented for both streaming methods compared to the 'no streaming' baseline cases at $U_\infty = 10$ m/s. Separate baseline cases were recorded for each transducer due to the differences in geometry discussed in Section IV.B. Due to unexpected electromagnetic interference between the transducers and the flush-mounted microphones, it was not possible to acquire surface pressure fluctuation data for the 'streaming on' cases. Future iterations of these experiments will address this issue, either by shielding the transducers and/or using remote sensing techniques.

Figure 6 displays the pressure coefficient variation along the centre of the plate for the two transducers. The pressure

coefficient was calculated as the ratio between pressure forces and inertial forces at each pressure tap location:

$$C_p = \frac{p - p_\infty}{\frac{1}{2}\rho U_\infty^2} \tag{1}$$

with p measured at each streamwise location, p_∞ measured at the inlet and the air density taken to be $\rho = 1.225$ kg/m^3. The baseline C_p is typical for a flat plate, as there is clearly an absence of any pressure gradient along the streamwise direction [32]. In both transducer cases, the effect of acoustic streaming on the static pressure distribution appears to be negligible.

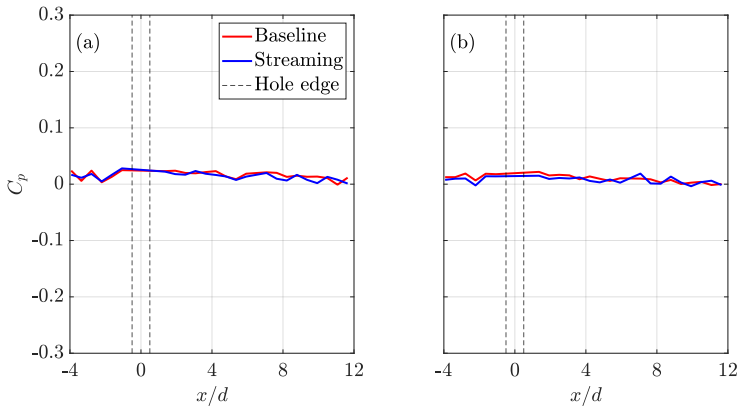

Fig. 6 Streamwise pressure coefficient distribution for the (a) Langevin horn and (b) focussed array case.

Figure(s) 7 and 8 show the normalised mean velocity profiles ($\bar{U}/U_\infty$) for the Langevin horn and focussed array streaming cases respectively. The baseline profile is representative of a turbulent boundary layer. Figure(s) 7a and 8a shows there is no upstream effect of the streaming on the boundary layer profile. Directly over the hole however ($x/d = 0$), there is an increase in mean velocity for both transducers (Figs. 7b and 8b). The height at which the maximum difference between streaming and baseline occurs is $z/\delta = 0.11$ for the Langevin horn, compared to $z/\delta = 0.02$ for the focussed array. At $x/d = 0.5$ there is a small reduction in mean velocity for the Langevin horn case (Fig. 7c), and by $x/d = 1.5$ the flow fully recovers from the streaming perturbation (Fig. 7d). The focussed array case shows no such reduction, with Figs. 8c and 8d displaying no change between the streaming case and the baseline.

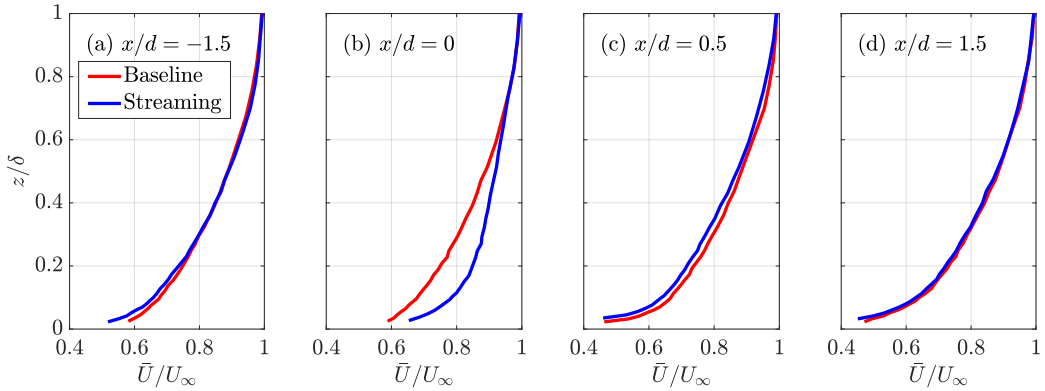

Fig. 7 Boundary layer profiles for the Langevin horn case.

The fluctuations in the hot-wire anemometry data can give an indication of the turbulent energy content within the boundary layer. Figure(s). 9 and 10 show the turbulence intensity, calculated as,

$$\mathrm{TI} = \frac{u'}{U_\infty}, \tag{2}$$

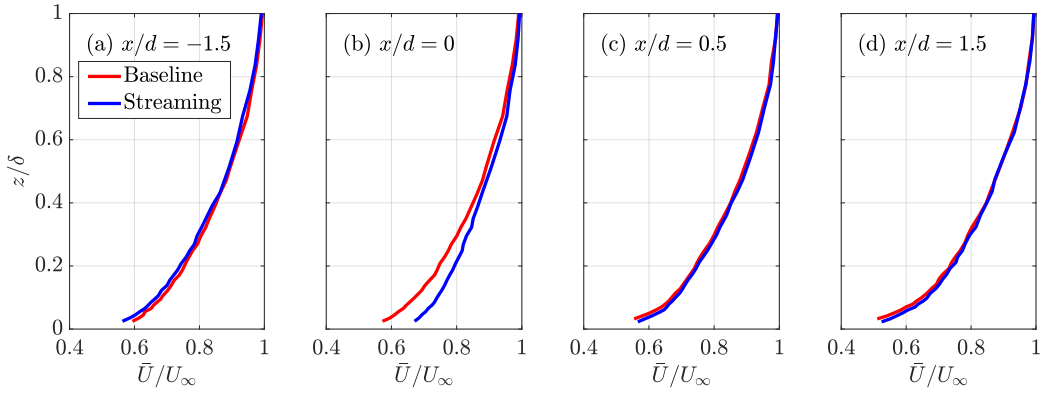

Fig. 8 Boundary layer profiles for the focussed array case.

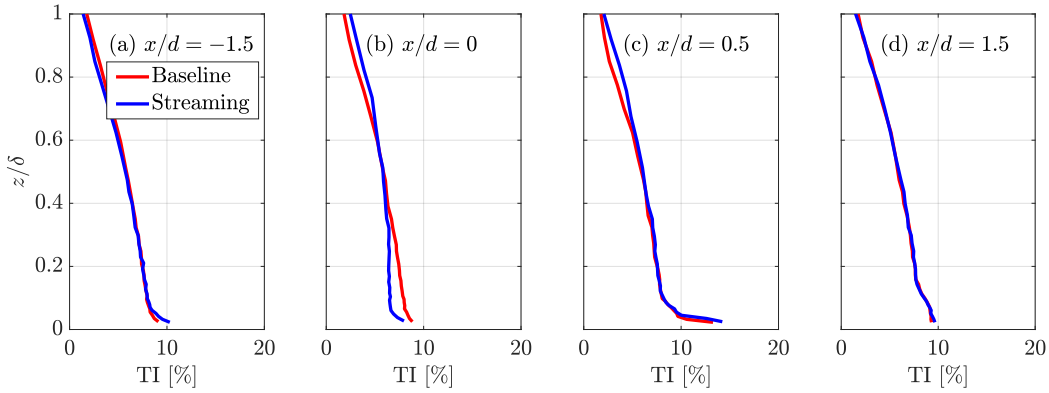

Fig. 9 Turbulent intensity profiles for the Langevin horn case.

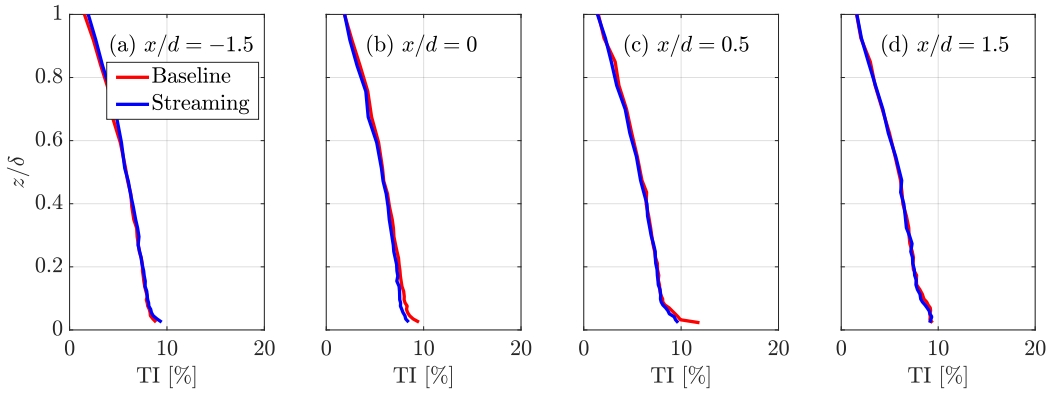

Fig. 10 Turbulent intensity profiles for the focussed array case.

where u' is the root-mean-square (RMS) of the velocity fluctuation, for the Langevin horn and focussed array, respectively. As with the mean velocity profiles, upstream of the streaming location shows little change between streaming and baseline (Figs. 9a and 10a). Figure 9b shows there is a reduction in turbulence intensity for the Langevin horn case at the streaming location ($x/d = 0$) in the lower half of the boundary layer ($z/\delta < 0.5$). The greatest reduction is seen at $z/\delta = 0.06$. In the upper half of the boundary layer ($z/\delta > 0.5$) there is an increase in turbulence intensity due to the streaming. The streaming induced by the focussed array case yields a less significant change in turbulence intensity

(Fig. 10b). In this case there is still a reduction lower in the boundary layer: the greatest reduction here occurs at the lowest measured point ($z/\delta = 0.02$). Further downstream at $x/d = 0.5$ sees a similar increase in turbulence intensity for $z/\delta > 0.5$ for the Langevin horn, and little difference between baseline and streaming cases in the lower half of the boundary layer (Fig. 9c). At the same streamwise location, the focussed array streaming has a negligible effect on the turbulence intensity except at the very lowest measured point, where there is a reduction (Fig. 10c). Figure(s) 9d and 10d show no change in turbulence intensity between the streaming and baseline cases for both transducers at $x/d = 1.5$.

Figure(s) 11 and 12 show the normalised mean velocities in both xz and yz planes directly over the transducer hole for the Langevin horn and focussed array respectively, as measured during the hot-wire anemometry scans depicted in Fig. 4b. Results are presented at five boundary layer heights, with the baseline cases showing no change in mean velocity over the measured points in either the streamwise (xz) or spanwise (yz) planes. The streaming cases for both transducers show an increase in mean velocity directly over the centre of the hole, particularly at the lowest measured boundary layer heights. The velocity profiles are effectively symmetrical about the centre of the hole ($x/d = y/d = 0$), with the velocity decreasing towards the baseline magnitudes at the hole edges ($x/d = y/d = \pm 0.5$). The streaming induced by the Langevin horn (Fig. 11) causes a more significant increase in mean velocity than that of the focussed array (Fig. 12). The increase in mean velocity due to the acoustic streaming reduces at increasing z/δ values (i.e. higher in the boundary layer). Thus, Fig. 11 shows that at $z/\delta = 0.96$ the effects of the Langevin horn streaming are no longer visible, while Fig. 12 indicates that the streaming flow from the focussed array does not affect the mean velocity above $z/\delta = 0.5$.

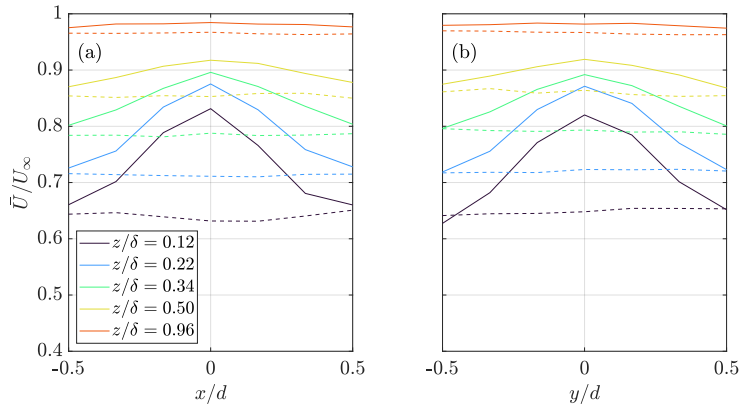

Fig. 11 Baseline (dashed) and streaming (solid) mean velocities in the (a) xz and (b) yz planes at various z/δ positions for the Langevin horn case.

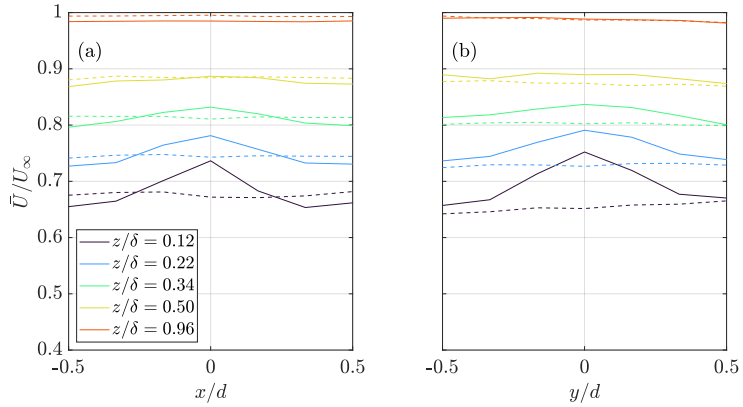

Fig. 12 Baseline (dashed) and streaming (solid) mean velocities in the (a) xz and (b) yz planes at various z/δ positions for the focussed array case.

Figure(s) 13 and 14 display the turbulence intensity results across the transducer hole at five boundary heights in the xz and yz planes for the Langevin horn and focussed array streaming cases, respectively. The baseline cases show

a constant turbulence intensity across the hole at all boundary layer heights, whereas both streaming cases cause a reduction in velocity fluctuations. As with the mean velocity results in Figs. 11 and 12, the turbulence intensity reduction due to the streaming from both transducers is greatest at the centre of the hole, and the profiles are symmetrical about this location. The most significant reduction occurs at the lowest measured height ($z/\delta = 0.12$), with the magnitude of the reduction decreasing at greater values of z/δ. Figure 13 shows the streaming flow from the Langevin horn has a larger effect on the turbulence intensity than that of the focussed array (Fig. 14). At BL heights above $z/\delta = 0.5$ there is no significant difference between the focussed array streaming case and the baseline (Fig. 14), whereas the effect of the streaming from the Langevin horn is still visible at $z/\delta = 0.5$ (Fig. 13). At $z/\delta = 0.96$ there is no change between the streaming cases and the baseline.

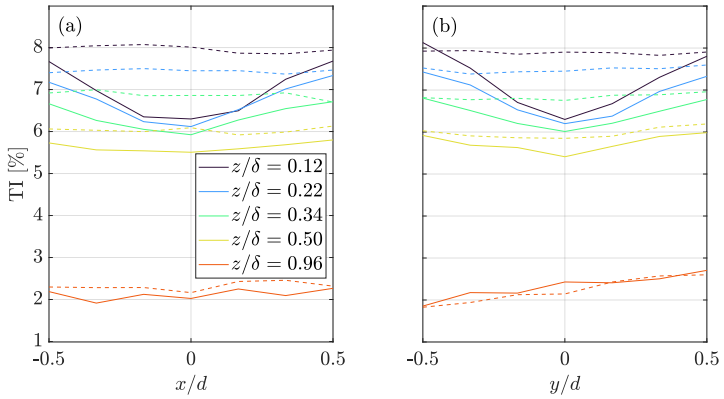

Fig. 13 Baseline (dashed) and streaming (solid) turbulence intensities in the (a) xz and (b) yz planes at various z/δ positions for the Langevin horn case.

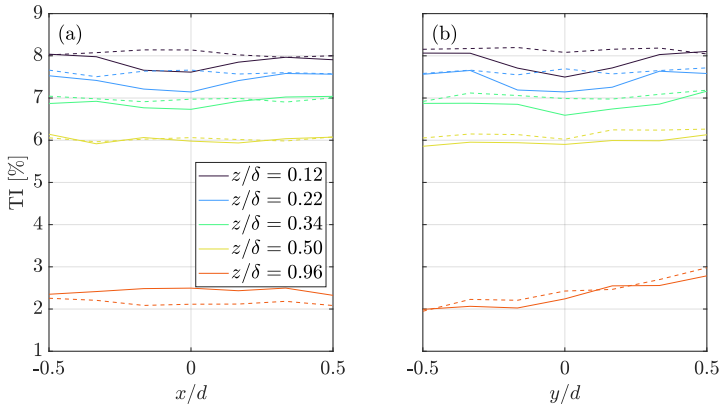

Fig. 14 Baseline (dashed) and streaming (solid) turbulence intensities in the (a) xz and (b) yz planes at various z/δ positions for the focussed array case.

The effect of the Langevin horn was greater than that of the array, so the following analysis is performed on the Langevin horn only. Figure 15 displays the baseline and streaming case PSD levels at two boundary layer heights ($z/\delta = 0.12$ and $z/\delta = 0.22$) over the centre of the hole ($x/d = y/d = 0$). The PSD level is calculated by:

$$\text{PSD} = 10\log_{10}(\phi_{uu}) \tag{3}$$

with ϕ_{uu} (the power spectral density of the velocity fluctuations) computed using Welch's method in MATLAB [33]. From here for ease the PSD level is referred to as PSD. The baseline velocity PSD is typical for that of a turbulent boundary layer over a flat plate [3]. It can be seen that the streaming causes a reduction in energy content of up to 3 dB

between 10 Hz and 2000 Hz at both boundary layer heights. The magnitude of the reduction is less significant above 2000 Hz, with a reduction of approximately 1.5 dB.

Figure 16 shows a contour plot of the ΔPSD, given as:

$$\Delta\text{PSD} = \text{PSD}_{streaming} - \text{PSD}_{baseline} \tag{4}$$

for the full height of the boundary layer at the streaming location ($x/d = y/d = 0$). Acoustic streaming induced by the Langevin horn causes a reduction in the turbulent energy content of up to 3 dB across frequencies between 10 Hz and 8 kHz in the lower half of the boundary layer ($z/\delta < 0.4$) at the streaming location. At $z/\delta > 0.6$, further up in the boundary layer, there is an increase in energy between 0.5 dB and 2 dB across all frequencies.

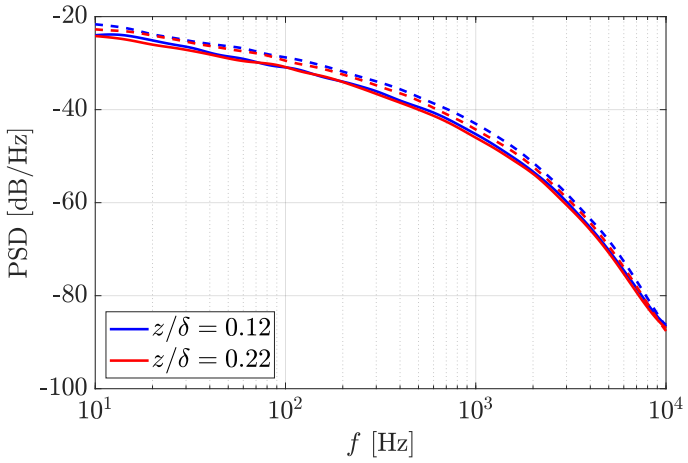

Fig. 15 PSDs for baseline (dashed) and Langevin horn streaming (solid) at $x/d = y/d = 0$.

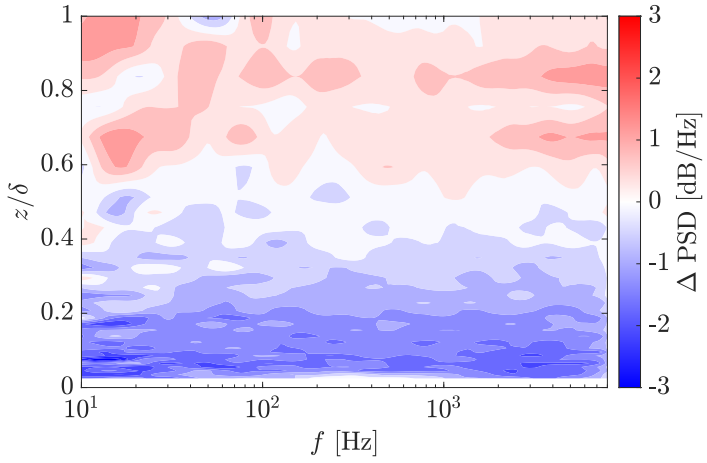

Fig. 16 ΔPSD contour plot for the Langevin horn at $x/d = y/d = 0$.

It is clear there is a difference between the two streaming methods employed. One possible explanation for the more significant effect of the Langevin horn compared to that of the focussed array, was the differences in geometry between the two setups. The surface of the plate remained effectively flat with the Langevin horn, however in the case of the focussed array the ability of the acoustic streaming to affect boundary layer structures was potentially limited by the presence of the cavity. It could be conceived that with such a feature, the flow could be sucked beneath the plate through the hole, opposing any streaming flows generated by the transducer, and thus reducing the effects of the streaming flows on any boundary layer structures. Another possible factor was the difference in the size of the focal region in the

acoustic fields. Recall, Figure 2 shows that the size of the focal region of the array was smaller than that of the Langevin horn, which would result in acoustic streaming that had a lower volumetric flow rate, however this would require further investigation.

VI. Conclusions

The authors present a novel method of boundary layer manipulation through the use of bulk-driven acoustic streaming induced by high powered ultrasonic transducers. Two transduction methods were used to perturb a turbulent boundary layer over a flat plate, namely Langevin horns and a focussed array of parking sensor transducers. They operate at 26 kHz and 40 kHz respectively, and can produce sound pressure levels of up to 167 dB. The acoustic streaming flows from both transducers caused an increase in the mean velocity within the boundary layer at the transducer location, measured using hot-wire anemometry. A reduction in turbulence intensity in the lower half of the boundary layer was observed, with a slight increase in the upper half. The acoustic streaming from the Langevin horn had a more significant effect on the boundary layer compared to that of the focussed array, possibly owing to the presence of a cavity in the focussed array setup. Further investigation has shown that the streaming flows induced by the Langevin horn result in reductions in turbulent energy content of up to 3 dB in the lower half of the boundary layer over a wide range of frequencies.

References

[1] Howe, M. S., "Noise produced by a sawtooth trailing edge," *Journal of the Acoustical Society of America*, Vol. 90, No. 1, 1991, pp. 482–487. https://doi.org/10.1121/1.401273.

[2] Lyu, B., Azarpeyvand, M., and Sinayoko, S., "Prediction of noise from serrated trailing edges," *Journal of Fluid Mechanics*, Vol. 793, 2016, pp. 556–588. https://doi.org/10.1017/jfm.2016.132.

[3] Showkat Ali, S. A., Azarpeyvand, M., Szoke, M., and Ilário Da Silva, C. R., "Boundary layer flow interaction with a permeable wall," *Physics of Fluids*, Vol. 30, No. 8, 2018. https://doi.org/10.1063/1.5043276.

[4] Bowen, L., Celik, A., Zhou, B., Westin, M. F., and Azarpeyvand, M., "The effect of leading edge porosity on airfoil turbulence interaction noise," *The Journal of the Acoustical Society of America*, Vol. 152, No. 3, 2022, pp. 1437–1448. https://doi.org/10.1121/10.0013703.

[5] Afshari, A., Azarpeyvand, M., Dehghan, A. A., Szőke, M., and Maryami, R., "Trailing-edge flow manipulation using streamwise finlets," *Journal of Fluid Mechanics*, Vol. 870, No. June 2016, 2019, pp. 617–650. https://doi.org/10.1017/jfm.2019.249.

[6] Gstrein, F., Zang, B., and Azarpeyvand, M., "Investigations on the Application of Various Surface Treatments for Trailing Edge Noise Reduction on a Flat Plate," *AIAA Aviation and Aeronautics Forum and Exposition, AIAA AVIATION Forum 2021*, 2021, pp. 1–17. https://doi.org/10.2514/6.2021-2263.

[7] Lee, C., Hong, G., Ha, Q. P., and Mallinson, S. G., "A piezoelectrically actuated micro synthetic jet for active flow control," *Sensors and Actuators, A: Physical*, Vol. 108, No. 1-3, 2003, pp. 168–174. https://doi.org/10.1016/S0924-4247(03)00267-X.

[8] Park, J., and Choi, H., "Effects of uniform blowing or suction from a spanwise slot on a turbulent boundary layer flow," *Physics of Fluids*, Vol. 11, No. 12, 1999, pp. 3856–3859. https://doi.org/10.1063/1.870245.

[9] Szoke, M., Fiscaletti, D., and Azarpeyvand, M., "Uniform flow injection into a turbulent boundary layer for trailing edge noise reduction," *Physics of Fluids*, Vol. 32, No. 8, 2020. https://doi.org/10.1063/5.0013461, URL https://doi.org/10.1063/5.0013461.

[10] Reynolds, G. A., and Saric, W. S., "Experiments on the stability of the flat-plate boundary layer with suction," *AIAA Journal*, Vol. 24, No. 2, 1986, pp. 202–207. https://doi.org/10.2514/3.9246.

[11] Antonia, R. A., Zhu, Y., and Sokolov, M., "Effect of concentrated wall suction on a turbulent boundary layer," *Physics of Fluids*, Vol. 7, No. 10, 1995, pp. 2465–2474. https://doi.org/10.1063/1.868690.

[12] Wolf, A., Lutz, T., Wurz, W., Kramer, E., and Stalnov, O., "Trailing edge noise reduction of wind turbine blades by active flow control," *Wind Energy*, Vol. 2, No. March 2014, 2013, pp. 1–20. https://doi.org/10.1002/we.

[13] Feng, Z. P., Bing, L. A., and Jun, W. J., "Flow structures in flat plate boundary layer induced by pulsed plasma actuator," *Science China Technological Sciences*, Vol. 53, No. 10, 2010, pp. 2772–2782. https://doi.org/10.1007/s11431-010-4100-7.

[14] Rayleigh, L., "On the Circulation of Air observed in Kundt's Tubes, and on some Allied Acoustical Problems," *The Royal Society Publishing*, 1884.

[15] Schlichting, H., "Berechnung ebener periodischer Grenzschichtstromungen," *Phys. z.*, Vol. 33, 1932, pp. 327–335.

[16] Spengler, J. F., Coakley, W. T., and Christensen, K. T., "Microstreaming Effects on Particle Concentration in an Ultrasonic Standing Wave," *AIChE Journal*, Vol. 49, No. 11, 2003, pp. 2773–2782. https://doi.org/10.1002/aic.690491110.

[17] Spengler, J. F., and Coakley, W. T., "Ultrasonic trap to monitor morphology and stability of developing microparticle aggregates," *Langmuir*, Vol. 19, No. 9, 2003, pp. 3635–3642. https://doi.org/10.1021/la026798c.

[18] Vainshtein, P., Fichman, M., and Gutfinger, C., "Acoustic enhancement of heat transfer between two parallel plates," *International Journal of Heat and Mass Transfer*, Vol. 38, No. 10, 1995, pp. 1893–1899. https://doi.org/10.1016/0017-9310(94)00299-B.

[19] Loh, B.-G., Hyun, S., Ro, P. I., and Kleinstreuer, C., "Acoustic streaming induced by ultrasonic flexural vibrations and associated enhancement of convective heat transfer," *The Journal of the Acoustical Society of America*, Vol. 111, No. 2, 2002, pp. 875–883. https://doi.org/10.1121/1.1433811.

[20] Muller, P. B., Barnkob, R., Jensen, M. J. H., and Bruus, H., "A numerical study of microparticle acoustophoresis driven by acoustic radiation forces and streaming-induced drag forces," *Lab on a Chip*, Vol. 12, No. 22, 2012, pp. 4617–4627. https://doi.org/10.1039/c2lc40612h.

[21] Eckart, C., "Vortices and streams caused by sound waves," *Physical Review*, Vol. 73, No. 1, 1948, pp. 68–76. https://doi.org/10.1103/PhysRev.73.68.

[22] Nyborg, W. L., "Acoustic Streaming due to Attenuated Plane Waves," *Journal of the Acoustical Society of America*, Vol. 25, No. 1, 1953, pp. 68–75. https://doi.org/10.1121/1.1907010.

[23] Nyborg, W. L., "Acoustic Streaming near a Boundary," *Journal of the Acoustical Society of America*, Vol. 30, No. 4, 1958, pp. 329–339. https://doi.org/10.1121/1.1909587.

[24] Westervelt, P. J., "The Theory of Steady Rotational Flow Generated by a Sound Field," *Journal of the Acoustical Society of America*, Vol. 25, No. 1, 1953, pp. 60–67. https://doi.org/10.1121/1.1907009.

[25] Stuart, J., "Double boundary layers in oscillatory viscous flow," *Journal of Fluid Mechanics*, Vol. 24, 1966, pp. 673–687. https://doi.org/10.1017/S0022112066000910.

[26] Lighthill, J., "Acoustic streaming," *Theoretical and Computational Fluid Dynamics*, Vol. 10, No. 1-4, 1978, pp. 349–356. https://doi.org/10.1007/s001620050068.

[27] Hasegawa, K., Qiu, L., Noda, A., Inoue, S., and Shinoda, H., "Electronically steerable ultrasound-driven long narrow air stream," *Applied Physics Letters*, Vol. 111, No. 6, 2017. https://doi.org/10.1063/1.4985159, URL http://dx.doi.org/10.1063/1.4985159.

[28] Hasegawa, K., Yuki, H., and Shinoda, H., "Curved acceleration path of ultrasound-driven air flow," *Journal of Applied Physics*, Vol. 125, No. 5, 2019, pp. 1–7. https://doi.org/10.1063/1.5052423, URL http://dx.doi.org/10.1063/1.5052423.

[29] Rubinetti, D., Weiss, D. A., Wahlen, A., and Müller, J., "Numerical Modeling and Validation Concept for Acoustic Streaming Induced by Ultrasonic Treatment," *2016 COMSOL Conference in Munich*, 2016, pp. 12–14. URL https://www.comsol.com/paper/download/357161/rubinetti_paper.pdf%0Ahttps://www.comsol.com/paper/numerical-modeling-and-verification-of-acoustic-streaming-induced-by-ultrasonic--38061.

[30] Zang, B., Mayer, Y. D., and Azarpeyvand, M., "A note on the pressure–velocity correlation and coherence normalisation," *Experiments in Fluids*, Vol. 61, No. 8, 2020, pp. 1–7. https://doi.org/10.1007/s00348-020-03019-0, URL https://doi.org/10.1007/s00348-020-03019-0.

[31] Ali, S. A. S., "Flow over and past porous surfaces," Ph.D. thesis, University of Bristol, 2018.

[32] Bearman, P. W., "An investigation of the forces on flat plates normal to a turbulent flow," *Journal of Fluid Mechanics*, Vol. 46, No. 1, 1971, pp. 177–198. https://doi.org/10.1017/S0022112071000478.

[33] Welch, P. D., "The Use of Fast Fourier Transform for the Estimation of Power Spectra: A Method Based on Time Averaging Over Short, Modified Periodograms," *IEEE Transactions on Audio and Electroacoustics*, Vol. 15, No. 2, 1967, pp. 70–73. https://doi.org/10.1109/TAU.1967.1161901.